Catalysis Science & Technology

Accepted Manuscript

This is an *Accepted Manuscript*, which has been through the Royal Society of Chemistry peer review process and has been accepted for publication.

Accepted Manuscripts are published online shortly after acceptance, before technical editing, formatting and proof reading. Using this free service, authors can make their results available to the community, in citable form, before we publish the edited article. We will replace this *Accepted Manuscript* with the edited and formatted *Advance Article* as soon as it is available.

You can find more information about *Accepted Manuscripts* in the Information for Authors.

Please note that technical editing may introduce minor changes to the text and/or graphics, which may alter content. The journal's standard Terms & Conditions and the Ethical guidelines still apply. In no event shall the Royal Society of Chemistry be held responsible for any errors or omissions in this *Accepted Manuscript* or any consequences arising from the use of any information it contains.

ROYAL SOCIETY OF CHEMISTRY

www.rsc.org/catalysis

Catalysis Science & Technology

Dynamic Article Links►

Paper

Cite this: DOI: 10.1039/c0xx00000x

www.rsc.org/xxxxxx

Alkaline-assisted Ni nanocatalysts with largely enhanced low-temperature activity toward CO_2 methanation

Jie Liu,[a] Weihan Bing,[a] Xiaoge Xue,[a] Fei Wang,[a] Bin Wang,[b] Shan He,*[a] Yingkui Zhang,[a] Min Wei*[a]

Received (in XXX, XXX) Xth XXXXXXXXX 20XX, Accepted Xth XXXXXXXXX 20XX

DOI: 10.1039/b000000x

Abstract: The CO_2 methanation reaction is a promising approach for the chemical transformation of carbon dioxide into useful fuels or products. The key challenge at present relies on the design and exploration of non-noble metal catalysts so as to achieve a high activity at low reaction temperature. In this work, we have obtained alkaline-assisted Ni nanocatalysts supported on Mg/Al mixed metal oxides (denoted as $Ni_x/Mg_{2-x}Al$-MMO) derived from Ni-Mg-Al hydrotalcite precursors. The catalytic performance toward CO_2 methanation was studied in detail, and the best low-temperature reaction activity was obtained over Ni/MgAl-MMO (CO_2 conversion: 97.9%; selectivity: 97.5%; 250 °C). By establishing the correlation between the catalytic performance and the alkaline site structure, it is found that Ni nanoparticle and MgO base site at the interface serve as dual active center to cooperatively catalyze CO_2 methanation, resulting in low-temperature reaction activity. Moreover, *in situ* diffuse reflectance Fourier transform infrared spectroscopy (*in situ* DRIFTS) demonstrates that MgO acts as the active site for CO_2 activation to give carbonate/hydrocarbonate species, while Ni provides H-species for further hydrogenation of intermediates. Therefore, this work rationalizes the significant influence of alkaline-assisted Ni nanoparticles on CO_2 methanation, which provides a promising heterogeneous catalyst for this reaction.

1. Introduction

The chemical transformation of CO_2 from industrial exhaust gas (e.g., H_2-rich coke oven gas,[1] COG) into value-added chemical fuels is of vital importance for promoting energy regeneration and solving environmental problems.[2] Among them, the hydrogenation of CO_2 to methane is one of the most promising CO_2 conversion processes.[3] Currently, studies for CO_2 methanation have been focused on the design of supported non-noble catalysts with enhanced low-temperature activity and stability.[4] It has been widely accepted that introduction of alkaline species onto the support is an effective way to increase catalytic activity and stability.[5] Previous investigations mainly involve changing the category and quantity of alkali species in support so as to obtain enhanced catalytic activity. As is well known, the alkaline is substantially determined by alkaline sites structure/property on the surface (e.g., type, strength, concentration, dispersion and stability).[6] Park *et al*. proposed that the alkaline site can initiate the methanation reaction by binding a CO_2 molecule to form carbonate species, followed by hydrogenation with dissociated hydrogen to produce methane based on the DFT calculations.[7] However, experimental evidence concerning the influence of alkaline site structure on catalytic performance is rather lacking, and how to create desirable alkaline sites remains a challenge. Therefore, a systematic research for alkaline site structure and its catalysis mechanism would be valuable for rational design of new catalysts with largely improved catalytic performance.

Layered double hydroxides[8] (LDHs) are a class of two-dimensional (2D) anionic clays consisting of positively charged host layers and exchangeable interlayer anions, which can be generally expressed by the formula $[M^{2+}_{1-x}M^{3+}_x(OH)_2](A^{n-})_{x/n}\cdot mH_2O$. An unique structural characteristic of LDHs materials is that the M^{2+} and M^{3+} cations are distributed in a highly-ordered state in the hydroxide layers. Recently, considerable interest has been focused on LDH materials as catalysts, catalyst supports or precursors by virtue of their versatility in chemical composition and structural architecture.[9] Compared with traditional supported catalysts, the LDH-based catalysts show the following advantages: (1) if the LDH precursor contains transition metal ions, they can be *in situ* reduced to give catalytically-active metal nanoparticles anchoring to a so-called mixed metal oxide phase, with a high dispersion and stability; (2) if a proportion of alkaline elements (e.g., Mg) is further introduced into the LDHs precursor, a tunable alkaline site structure can be obtained. Therefore, it is a promising strategy for fabricating alkaline-assisted metal nanocatalysts with enhanced cooperative catalysis.

In this work, alkaline-assisted Ni nanocatalysts supported on Mg/Al mixed metal oxides (denoted as $Ni_x/Mg_{2-x}Al$-MMO) were successfully prepared by a facile reduction treatment upon the $Ni_xMg_{2-x}Al$-LDH precursors, and their catalytic performances toward CO_2 methanation were studied in detail. The Ni/MgAl-MMO catalyst shows the best catalytic behavior with a

[a] *State Key Laboratory of Chemical Resource Engineering, Beijing University of Chemical Technology, Beijing, 100029, China*

[b] *Beijing Research Institute of Chemical Industry, Sinopec Group, Beijing 100013, P. R. China*

E-mail:vh30@163.com; weimin@mail.buct.edu.cn; Fax: +86-10-64425385; Tel: +86-10-64412131

Electronic supplementary information (ESI) available. See DOI: 10.1039/c0xx00000x

Catalysis Science & Technology Accepted Manuscript

CO_2 conversion of 97.9 % and selectivity of 97.5 % (250 °C), which serves as a promising candidate for the substitution of noble metal catalysts. Based on the results of XRD, HRTEM, H_2 chemisorption and *in situ* CO-FTIR, it is found that the TOF value with respect to the exposed Ni atom (TOF_{Ni}) increases gradually with the increment of the density of MgO base sites, although these $Ni_x/Mg_{2-x}Al$-MMO catalysts show rather close average particle size of Ni. This verifies that the cooperative catalysis between Ni sites and MgO base sites accounts for the enhanced low-temperature reaction activity. Moreover, *in situ* DRIFTS reveals that MgO participates in this reaction by effectively activating CO_2, while Ni provides H-species for further hydrogenation of activated CO_2. This work demonstrates a successful paradigm for the development of tunable base sites, which play a key role in obtaining an optimal cooperative effect in CO_2 methanation.

2. Experimental Section

2.1 Materials

$Ni(NO_3)_2{\cdot}6H_2O$, $Mg(NO_3)_2{\cdot}6H_2O$ and $Al(NO_3)_3{\cdot}9H_2O$ were purchased from Sigma-Aldrich. Other chemicals including NaOH, Na_2CO_3 were purchased from the Beijing chemical Co., LTD., and deionized water was used in all the experimental processes.

2.2 Synthesis of $Ni_xMg_{2-x}Al$-LDH precursors and $Ni_x/Mg_{2-x}Al$-MMO catalysts

The $Ni_xMg_{2-x}Al$-LDH precursors with tunable compositions were synthesized by using a method that involves separate nucleation and aging steps (SNAS) developed in our laboratory.[10] Typically, $Ni(NO_3)_2{\cdot}6H_2O$, $Mg(NO_3)_2{\cdot}6H_2O$ and $Al(NO_3)_3{\cdot}9H_2O$ with various molar ratios of Ni^{2+}/Mg^{2+} were dissolved in 100 mL of deionized water to give a solution with a total cationic concentration of 0.15 M (solution A). A certain amount of NaOH and Na_2CO_3 were dissolved together to obtain 100 mL of a base solution (solution B: $[CO_3^{2-}] = 2.0\ [M^{3+}]$, $[OH^-] = 1.8\ ([M^{2+}]+[M^{3+}])$). Solution A and B were then mixed together at a steady rate of 3000 rpm for 1 min. The resulting suspension was aged in a sealed Teflon autoclave at 110 ℃ for 48 h. the obtained precipitate was washed thoroughly with water and ethanol and dried in an oven at 60 ℃ overnight. Finally, the obtained $Ni_xMg_{2-x}Al$-LDH precursor was reduced in a H_2/N_2 (1/9, *v*/*v*) stream at reduction temperature of 500 ℃ for 4 h, with a heating rate of 5 ℃/min. The reduction process results in the phase transformation from $Ni_xMg_{2-x}Al$-LDH to metallic Ni nanoparticles supported on MgO-Al_2O_3 mixed metal oxides (denoted as $Ni_x/Mg_{2-x}Al$-MMO).

2.3 Synthesis of Ni/CNT, Ni/Al_2O_3 and Ni/MgO catalysts

In order to carry out a comparison study, supported Ni catalysts on three substrates (carbon nanotubes CNTs, Al_2O_3, MgO) as reference samples were synthesized by impregnation method. In detail, the support (3.0 g) was dispersed into $Mg(NO_3)_2{\cdot}6H_2O$ solution (2.2230 g, 5.0 mL). After agitation for 3 h, the resulting slurry was dried at 60 ℃ for 4 h, followed by calcination in air at 400 ℃ for 3 h. Finally, the calcined sample was reduced in a H_2/N_2 (1/9, *v*/*v*) stream at 500 ℃ for 4 h, with an heating rate of 5 ℃/min, which was denoted as Ni/CNT, Ni/Al_2O_3 and Ni/MgO catalyst, respectively.

2.4 Characterization

X-ray diffraction (XRD) patterns of samples were obtained on a Rigaku XRD-6000 diffractometer, using Cu Kα radiation (λ = 0.154 nm) at 40 kV, 40 mA, a scanning rate of 10°/min, a step size of 0.02°/s, and a 2θ angle ranging from 3 to 70°. The morphology of the samples was investigated using a Zeiss Supra 55 scanning electron microscope (SEM) with an accelerating voltage of 20 kV. Metal elements analysis was analyzed using a Shimadzu ICPS-7500 inductively coupled plasma–atomic emission spectrometer (ICP−AES). Low-temperature N_2 adsorption-desorption experiments were carried out using the Quantachrome Autosorb-1C-VP instrument. Prior to N_2 adsorption, the sample was outgassed at 200 ℃ overnight to desorb moisture on the surface of the sample. The total specific surface area was evaluated from the multipoint Brunauer-Emmett-Teller (BET) method. High-resolution electron microscopy (HRTEM) observations were carried out on a JEM-2100 transmission electron microscope. Hydrogenation temperature programmed reduction (H_2-TPR) and hydrogenation temperature programmed desorption (H_2-TPD) were conducted in a quartz tube reactor on a Micromeritics ChemiSorb 2720 with a thermal conductivity detector (TCD). In a typical H_2-TPR process, 100 mg of a sample placed in a quartz tube reactor was first degassed under flowing argon at 400 ℃ for 2 h and cooled down to room temperature. Then a gaseous mixture of H_2 and Ar (1:9, *v*/*v*) was fed to the reactor at 50 mL/min. The temperature was raised to 700 ℃ at a heating rate of 10 ℃/min. For the H_2-TPD process, 100 mg of the reduced sample was first sealed and calcined in the reactor in the gaseous mixture of H_2 and Ar (1:9, *v*/*v*) at 400 ℃ for 1 h. Subsequently, the catalyst was purged in Ar at 500 ℃ for 30 min to remove excess hydrogen, then cooled down to 25 ℃ for readsorption of H_2; finally, the sample was conducted in a stream of argon with rate of 50 mL/min and a temperature ramp of 10 ℃/min to perform the TPD.

In situ Fourier-transformed infrared absorption spectroscopy of CO experiments were carried out in a quartz cell equipped with KBr windows allowing sample activation and successive measurements in the range 25–600 ℃, at a pressures as low as 10^{-4}. About 50 mg of the sample was pressed into a disk and activated in the same cell used for the measurement. FTIR spectra were collected with Nicolet 380 instrument spectrophotometer at a spectra resolution of 4 cm^{-1} and accumulation of 64 scans. After treatment in hydrogen at 400 ℃ for 1 h, the sample was purged in Ar at 500 ℃ for 30 min to remove excess hydrogen and then cooled to 50 ℃ and scanned to get a background record below a pressure of 2×10^{-4} Pa. Then the sample was exposed to a CO flow at 50 ℃ for another 120 min. Sample scanning for adsorbed CO was conducted after the pressure was reduced below 2×10^{-4} Pa again.

In situ diffuse reflectance Fourier transform infrared spectroscopy (*in situ* DRIFTS) was carried out on an *in situ* reaction cell. The spectra were collected in a Magna 6700 spectrometer equipped with a MCT narrow-band detector. The reaction gas mixture was introduced into the reaction cell via mass flow controllers. Prior to the experiments, the catalyst was heated up in a H_2/N_2 (1/9, *v*/*v*) stream to 500 ℃ for 2 h, and then cooled down to 170 ℃ for the background spectra collection. The methanation of CO_2 over the catalyst occurs with the introduction of $^{12}CO_2$-containing reaction gas mixture into the *in situ* cell.

Catalysis Science & Technology Accepted Manuscript

After the spectra signals reach up to saturation, the $^{12}CO_2$ gas is switched to $^{13}CO_2$ for a further spectra record.

2.5 Catalytic evaluation

The catalytic performance of the nickel-based catalysts was evaluated at atmospheric pressure in a fixed-bed quartz reactor with an interior diameter of 8 mm. The reactor was heated in a tube furnace equipped with a temperature controller, and all gases were monitored by calibrated mass flow controllers. Prior to the catalytic performance test, 0.5 g of catalyst was first pretreated in a gaseous mixture of H_2/N_2 (1/9, *v*/*v*) for 1 h with total gas flow of 100 mL/min at 500 ℃ with a heating rate of 5 ℃/min, and then cooled to 100 ℃ in nitrogen. Subsequently, a mixture of H_2, CO_2 and Ar (an internal standard) with a molar ratio of H_2 : CO_2 : Ar = 12 : 3 : 5 was introduced into the reactor with a total flux of 40 mL/min. The gas hourly space velocity (GHSV) was maintained at 2400 h^{-1}. The composition of the outlet gases was analyzed online using a GC-2014C gas chromatograph equipped with a TCD detector and FID detector. The CO_2 conversion (eq. 1) and CH_4 selectivity (eq. 2) are defined as follows:

$$\text{Conversion}_{CO_2}(\%) = (1 - \frac{S_{out(CO_2)} S_{in(Ar)}}{S_{in(CO_2)} S_{out(Ar)}}) \times 100 \quad (1)$$

$$\text{Selectivity}_{CH_4}(\%) = \frac{c_{(CH_4)}}{0.15 \times (\frac{S_{out(Ar)}}{S_{in(Ar)}} - \frac{S_{out(CO_2)}}{S_{in(CO_2)}})} \times 100 \quad (2)$$

where $S_{in(CO2)}$ and $S_{out(CO2)}$ are the peak areas of CO_2 in inlet and outlet gas determined by gas chromatograph; $S_{in(Ar)}$ and $S_{out(Ar)}$ are the peak areas of Ar in inlet and outlet gas; $c_{(CH4)}$ is the methane concentration in the outlet gas, which is calculated based on the external standard method.

Furthermore, the reaction rate (R) of $Ni_x/Mg_{2-x}Al$-MMO catalysts (eq. 3) is evaluated at a low reaction temperature (170 ℃) and low level of CO_2 conversion (<20%), to minimize the effects of transport and water inhibition. The reaction rate is calculated based on the following equation:

$$R = \frac{V \times C \times 10^{-3}}{m \times V_m} \quad (3)$$

where V refers the volume of CO_2 fed into the reaction per minute (mL min^{-1}); C is the conversion of CO_2 at 170 ℃; m denotes the weight of catalyst (g), and V_m is the molar volume of CO_2 (22.4 L mol^{-1}).

3. Result and discussion

3.1 Structural and morphological study of the catalysts

The $Ni_xMg_{2-x}Al$-LDH precursors with various Ni/Mg ratios (1/4, 2/3, 1/1 and 4/1) were synthesized *via* co-precipitation method. Their XRD patterns (Fig. S1A) show characteristic reflections at 2θ ~12°, ~24° and ~35°, which can be indexed to (003), (006) and (012) of an LDH phase, respectively.[11] After reduction of $Ni_xMg_{2-x}Al$-LDH precursors at 500 ℃ for 4 h, the corresponding Ni-based catalysts supported on Mg/Al mixed metal oxides (typically, crystalline MgO and amorphous Al_2O_3) were obtained (denoted as $Ni_x/Mg_{2-x}Al$-MMO). Fig. S1B shows the XRD patterns of the resulting $Ni_x/Mg_{2-x}Al$-MMO samples. Typical (200) and (220) reflection of face-centered MgO (JCPDS card no. 33-0664) at 2θ ~43° and 63° are observed in all these samples; while no characteristic reflection of metal Ni is found, indicative of a small particle size of the resulting Ni species. Moreover, the content of metal elements in these samples as well as the loading of Ni determined by inductively coupled plasma–atomic emission spectrometer (ICP−AES) are summarized in Table 1. The determined ratio of the total divalent to trivalent metal is maintained to be ~2:1 with Ni loading ranging from 17.2% to 57.8%, close to the nominal ones.

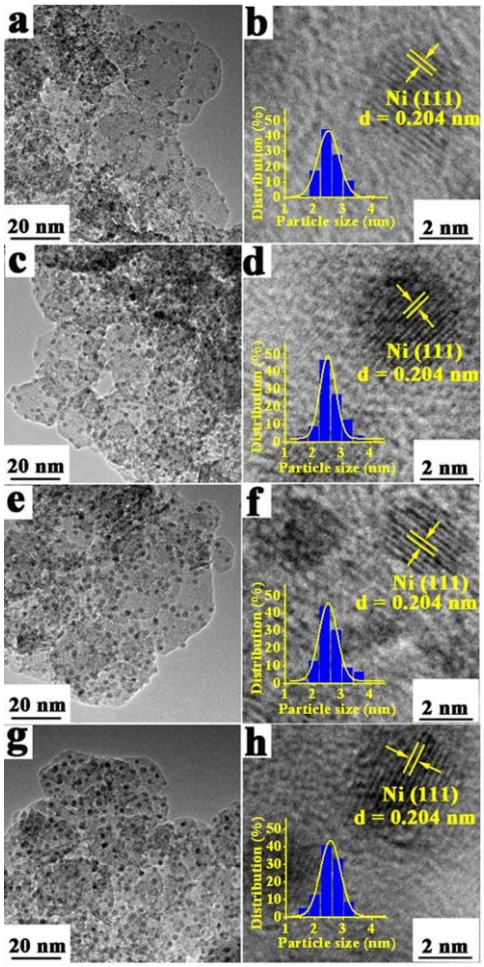

Fig.1 HRTEM images of the $Ni_x/Mg_{2-x}Al$-MMO samples: (a, b) $Ni_{0.4}/Mg_{1.6}Al$-MMO, (c, d) $Ni_{0.8}/Mg_{1.2}Al$-MMO, (e, f) Ni/MgAl-MMO, (g, h) $Ni_{1.6}/Mg_{0.4}Al$-MMO. The inset in (b), (d), (f) and (h) is the corresponding particle-size frequency distribution histogram (400 particles analyzed).

HRTEM measurements were performed to investigate the structure and distribution of Ni species in these $Ni_x/Mg_{2-x}Al$-MMO samples (Fig. 1). It is observed that Ni nanoparticles are highly dispersed within Mg/Al mixed metal oxides. Notably, with the enhancement of Ni/Mg molar ratio from 1/4 to 4/1, the density of Ni nanoparticles increases gradually, but their average size remains almost unchanged (~2.5 nm). The corresponding HRTEM images with a high magnification further reveal a characteristic lattice spacing of 0.204 nm for these nanoparticles, which is indexed to the (111) plane of fcc Ni. In addition, for comparison, three Ni particles supported on carbon nanotube (CNT), Al_2O_3 and MgO, respectively, were also prepared by the impregnation method, with a comparable Ni loading to the Ni/MgAl-MMO sample

Catalysis Science & Technology Accepted Manuscript

Table 1. Structural parameters of various samples

Catalysts	S_{BET} (m^2g^{-1})	Ni [a] (wt.%)	Molar ratio[a] (Ni/Mg/Al)	Ni dispersion [b] (%)	$n_{surface\ Ni}$ [b] (mmol g^{-1}_{cat})	$n_{CO2,Mg}$ [c] (mmol g^{-1}_{cat})	$n_{CO2,Al}$ [c] (mmol g^{-1}_{cat})	Mean Ni particle size by TEM (nm)
$Ni_{0.4}/Mg_{1.6}Al$-MMO	178	17.2	0.41/1.60/1.00	21.7	0.64	0.15	0.08	2.4±0.3
$Ni_{0.8}/Mg_{1.2}Al$-MMO	172	27.6	0.64/1.18/1.00	22.3	1.05	0.11	0.08	2.4±0.2
Ni/MgAl-MMO	161	36.9	0.98/1.00/1.00	21.3	1.34	0.09	0.07	2.5±0.3
$Ni_{1.6}/Mg_{0.4}Al$-MMO	157	57.8	1.56/0.40/1.00	19.8	1.94	0.03	0.07	2.5±0.3
Ni/CNT	412	36.6	—	9.80	0.61	—	—	7.1±1.6
Ni/Al_2O_3	41	37.4	—	11.2	0.71	—	0.07	5.2±1.0
Ni/MgO	33	37.8	—	14.6	0.95	0.12	—	4.0±0.8

[a]values determined by ICP−AES. [b]values calculated based on H_2 chemisorption.[2c,12] [c] values calculated based on CO_2-TPD.

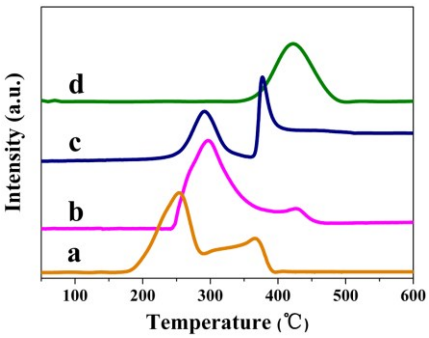

Fig. 2 H_2-TPR profiles of (a) Ni/CNT, (b) Ni/Al_2O_3, (c) Ni/MgO and (d) Ni/MgAl-MMO samples.

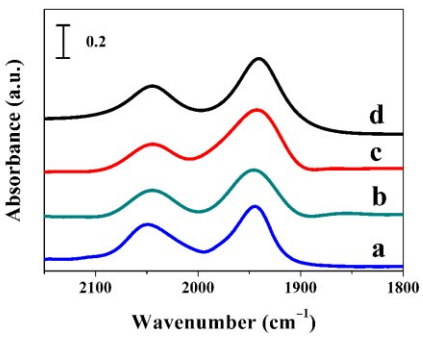

Fig. 3 *In situ* FTIR spectra of CO adsorption on the four $Ni_x/Mg_{2-x}Al$-MMO samples: (a) $Ni_{0.4}/Mg_{1.6}Al$-MMO, (b) $Ni_{0.8}/Mg_{1.2}Al$-MMO, (c) Ni/MgAl-MMO and (d) $Ni_{1.6}/Mg_{0.4}Al$-MMO.

(37%). The resulting Ni/CNT, Ni/Al_2O_3 and Ni/MgO catalysts are characterized by random packing of Ni nanoparticles with irregular shape and very broad particle size distribution (as shown in Fig. S2).

Hydrogen temperature programmed reduction (H_2-TPR) measurements were carried out to provide information on the redox properties of Ni/MgAl-MMO, Ni/CNT, Ni/Al_2O_3 and Ni/MgO, respectively (Fig. 2). For the reference samples of Ni/CNT, Ni/Al_2O_3 and Ni/MgO, two reduction peaks in the range 220–450 ℃ are observed, which are assigned to the reduction of bulk NiO (low temperature) and highly-dispersed NiO species (high temperature), respectively.[13] However, in the case of Ni/MgAl-MMO, only one unique and symmetric peak at a relatively high temperature (~435 ℃) is identified, indicating a relatively hard-to reduction Ni^{2+} species with a good uniformity in the LDH precursor.[14] This is related to the reason that Ni^{2+} is well diluted/isolated by Mg^{2+} and Al^{3+} cations in the LDH

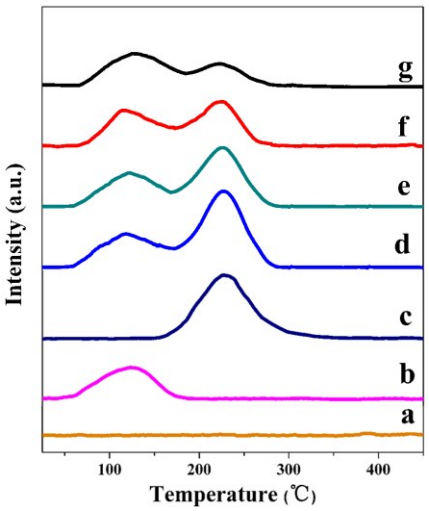

Fig. 4 CO_2-TPD profiles of the synthesized Ni samples: (a) Ni/CNT, (b) Ni/Al_2O_3, (c) Ni/MgO, (d) $Ni_{0.4}/Mg_{1.6}Al$-MMO, (e) $Ni_{0.8}/Mg_{1.2}Al$-MMO, (f) Ni/MgAl-MMO and (g) $Ni_{1.6}/Mg_{0.4}Al$-MMO.

lamellar. Moreover, the H_2 chemisorption capacities of the synthesized $Ni_x/Mg_{2-x}Al$-MMO, Ni/CNT, Ni/Al_2O_3 and Ni/MgO were further measured to obtain the specific Ni dispersion (Table 1). The four $Ni_x/Mg_{2-x}Al$-MMO samples show a comparable dispersion degree of ~20% owing to their rather close particle size, which is higher than that of Ni/CNT, Ni/Al_2O_3 and Ni/MgO samples (9.8%–14.6%). This is in accordance with the results of TEM. In addition, the surface structure of Ni particles in the four $Ni_x/Mg_{2-x}Al$-MMO samples was also studied by *in situ* infrared spectra of CO adsorption technique (as shown in Fig. 3). Two typical CO adsorption peaks (at ~2050 cm^{-1} and ~1950 cm^{-1}) with rather close intensity are observed, which are attributed to the linearly absorbed and bridge-bonded CO on Ni atoms,[15] respectively. This implies that the Ni particles in these four $Ni_x/Mg_{2-x}Al$-MMO samples possess similar surface structure.

The structure of base sites for $Ni_x/Mg_{2-x}Al$-MMO samples, Ni/CNT, Ni/Al_2O_3 and Ni/MgO was investigated by using CO_2-TPD (Figure 4). For the Ni/CNT sample, no obvious CO_2 desorption peak is observed, indicative of the absence of base sites on CNT support. In contrast, the Ni/Al_2O_3 sample shows one low-temperature peak at ~120 ℃, which is associated with weak base sites, while Ni/MgO displays one medium-temperature peak at ~220 ℃, corresponding to mediate strong base sites. Notably, all the four $Ni_x/Mg_{2-x}Al$-MMO samples exhibit two peaks at ~120 ℃ and 220 ℃, which are assigned to the adsorbed CO_2 on Al_2O_3

Catalysis Science & Technology Accepted Manuscript

phase and on MgO phase, respectively. Moreover, from $Ni_{1.6}/Mg_{0.4}Al$-MMO to $Ni_{0.4}/Mg_{1.6}Al$-MMO samples, the peak intensity (namely the capacity) of the adsorbed CO_2 on MgO increases gradually while that of the adsorbed CO_2 on Al_2O_3 remains at a comparable level. This is in consistent with the evolution of MgO and Al_2O_3 in these $Ni_x/Mg_{2-x}Al$-MMO samples. In addition, the amount of adsorbed CO_2 on MgO and Al_2O_3 in per gram of sample (denoted as $n_{CO2,Mg}$ and $n_{CO2,Al}$, respectively), is calculated by the CO_2-TPD (Table 1). For $Ni_x/Mg_{2-x}Al$-MMO samples, as the Mg/Ni molar ratio rises from 1/4 to 4/1, the value of $n_{CO2,Mg}/(n_{CO2,Mg}+n_{CO2,Al})$ increases gradually, indicating an enhanced medium-strong basic strength.

3.2 Evaluation of the catalytic behavior

The catalytic performances of the Ni/MgAl-MMO, Ni/CNT, Ni/Al_2O_3 and Ni/MgO catalyst toward the reaction of CO_2 methanation were studied. Fig. 5A displays CO_2 conversion as a function of reaction temperature. The values of T_{50}, corresponding to the temperature at which 50% conversion is obtained, are 195, 263, and 306 ℃ for Ni/MgAl-MMO, Ni/MgO and Ni/Al_2O_3, respectively. Moreover, it is found that the maximal levels of CO_2 conversion in the presence of Ni/Al_2O_3 and Ni/MgO catalyst are only 79.1 and 89.0% (at ~350 ℃), respectively. In the case of the Ni/MgAl-MMO catalyst, however, the CO_2 conversion exceeds 80% at 220 ℃ and reaches the maximal value (97.9%) at 250 ℃, which is far superior to the catalytic activity of supported noble-metal and Ni-based catalysts reported previously.[2c,9b,16] The Ni/MgAl-MMO clearly exhibits a significantly enhanced low-temperature activity for CO_2 methanation. Fig. 5B also shows the corresponding selectivity toward CH_4 as a function of reaction temperature over the Ni/MgAl-MMO, Ni/A_2O_3 and Ni/MgO catalyst. As can be seen, the selectivity to CH_4 over the three catalysts is satisfactory (>95%) at low temperature region; however, a slight decrease for the latter two samples above 300 ℃ is observed, possibly due to the occurrence of side reaction (e.g., reverse water-gas shift[17] and reforming reaction[18]). Notably, the sample of Ni/CNT almost suffers from an inactivation along the whole reaction temperature, which suggests that base site of support plays an important role in the catalytic process of CO_2 methanation.

The series of $Ni_x/Mg_{2-x}Al$-MMO catalysts provide a good model to investigate the effect of base sites on CO_2 methanation due to their parallel morphology and surface structure of Ni particles. To establish the structure–activity relationship, the reaction rates of $Ni_x/Mg_{2-x}Al$-MMO catalysts (listed in Table 2) were evaluated at low reaction temperature (170 ℃) and level of CO_2 conversion (<20%), to minimize the effects of transport and water inhibition. As shown in Fig. 6A, the correlation between reaction rate and Mg/Ni molar ratio for $Ni_x/Mg_{2-x}Al$-MMO catalysts displays a volcano shape along with the increase of Mg/Ni ratio, with the maximum reaction rate obtained for Ni/MgAl-MMO catalyst. This suggests that a cooperative catalysis between Ni sites and MgO base sites occurs in CO_2 methanation, which determines the catalytic activity. Subsequently, the TOF values with respect to the exposed Ni atom (TOF_{Ni}) are calculated for these samples, which increase in the following order: $Ni_{1.6}/Mg_{0.4}Al$-MMO (6.68×10^{-4} s^{-1}) < Ni/MgAl-MMO (10.8×10^{-4} s^{-1}) < $Ni_{0.8}/Mg_{1.2}Al$-MMO (12.0×10^{-4} s^{-1}) < $Ni_{0.4}/Mg_{1.6}Al$-MMO (13.8×10^{-4} s^{-1}). Although these $Ni_x/Mg_{2-x}Al$-MMO catalysts show very close average size and surface structure of Ni nanoparticles, their TOF_{Ni} values are rather different. Furthermore, the relationship between TOF_{Ni} value and the density of MgO base site for these $Ni_x/Mg_{2-x}Al$-MMO catalysts is studied (Fig. 6B), which shows a linear correlation. This further confirms the cooperative catalysis between Ni active site and MgO base site. The four $Ni_x/Mg_{2-x}Al$-MMO catalysts with very similar surface structure of

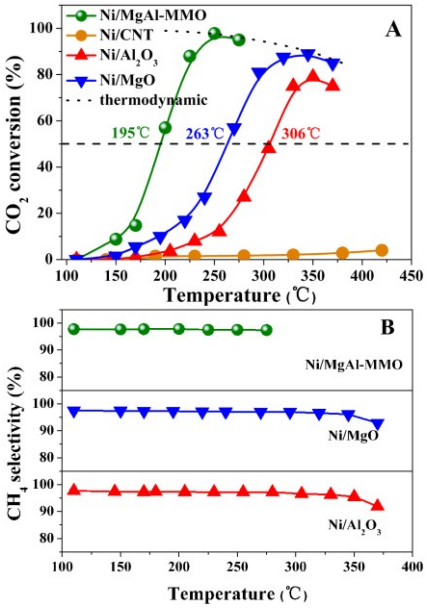

Fig. 5 (A) CO_2 methanation at steady state as a function of reaction temperature over the as-prepared Ni/MgAl-MMO, Ni/CNT, Ni/Al_2O_3 and Ni/MgO catalyst (GHSV: 2400 h^{-1}). (B) The corresponding selectivity toward CH_4 as a function of reaction temperature.

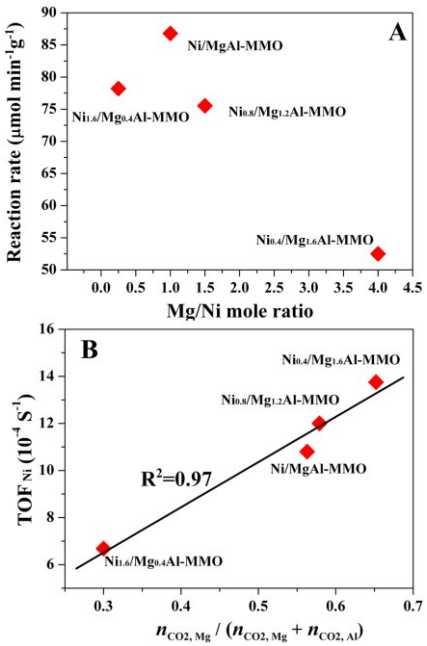

Fig. 6 (A) Correlation between reaction rate and Mg/Ni molar ratio for $Ni_x/Mg_{2-x}Al$-MMO catalysts (reaction conditions: 170 ℃, GHSV = 2400 h^{-1}, CO_2 conversion <20%). (B) Relationship between TOF_{Ni} and concentration of base sites in $Ni_x/Mg_{2-x}Al$-MMO catalysts.

Catalysis Science & Technology Accepted Manuscript

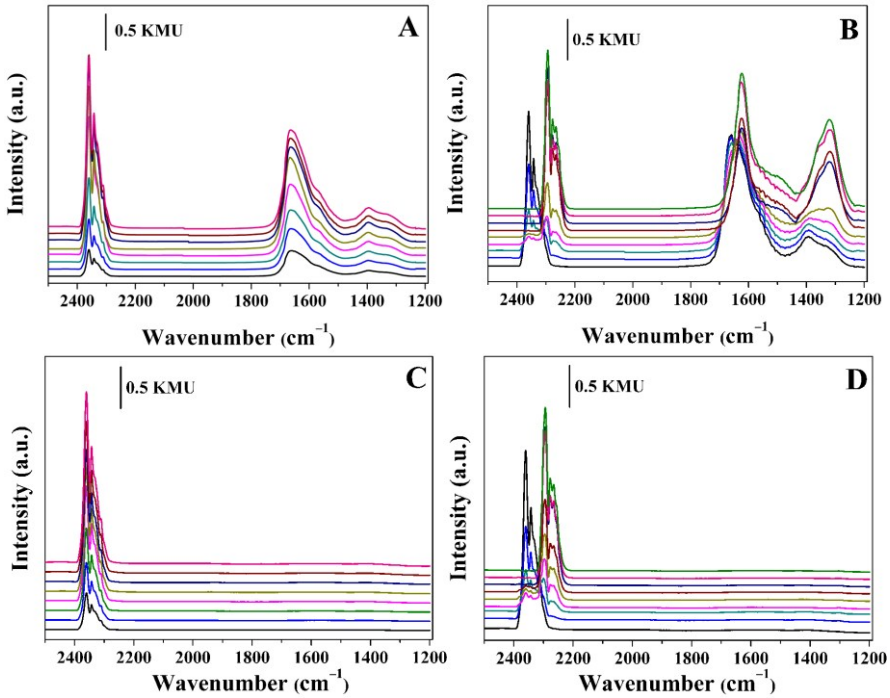

Fig. 7 DRIFT spectra recorded at 170 ℃ during 60 minwith$^{12}CO_2$ as reaction gas and subsequent 60 min reaction by introducing $^{13}CO_2$ over: (A, B) Ni/MgAl-MMO and (C, D) Ni/CNT . From bottom to top: (A, C) 0.5, 1.5, 3, 5, 10, 20, 40, 60 min; (B, D) 0, 0.5, 1.5, 3, 5, 10, 20, 40, 60 min.

Table 2. Catalytic performance of various catalysts[a]

Catalysts	T [b] (℃)	Conv.[b] (%)	Sel.[b] (%)	T_{50} (℃)	R[c](μmol min^{-1}g^{-1})	TOF_{Ni} (×10^{-4}s^{-1})
$Ni_{0.4}/Mg_{1.6}Al$-MMO	300	95.1	96.9	241	52.5	13.8
$Ni_{0.8}/Mg_{1.2}Al$-MMO	280	96.7	97.1	221	75.5	12.0
Ni/MgAl-MMO	250	97.9	97.5	195	86.7	10.8
$Ni_{1.6}/Mg_{0.4}Al$-MMO	270	96.5	97.1	210	78.2	6.68
Ni/CNT	—	—	—	—	—	—
Ni/Al_2O_3	350	79.1	95.5	306	16.1	3.75
Ni/MgO	345	89.0	96.1	263	29.5	5.22

[a] Reaction conditions: Catalyst (0.5 g), GHSV (2400 h^{-1}). [b] The results are obtained at the maximum conversion of CO_2. T_{50} refers to the reaction temperature at which a CO_2 conversion of 50% is obtained. [c] Values are calculated based on the amount of CO_2 per minute per gram of catalyst.

Ni nanoparticles show rather different TOF_{Ni} values, indicating the Ni−MgO interfacial site plays an important role in cooperatively catalyzing CO_2 methanation. By virtue of the tunable chemical composition of LDH precursors, a largely enhanced low-temperature activity is obtained over the catalyst of Ni/MgAl-MMO, which is likely attributed to the optimized cooperative effect between Ni and base site. In addition, the long-term catalytic stability of Ni/MgAl-MMO catalyst was also investigated. As shown in Fig. S3A, the CO_2 conversion remains almost constant during 100 h on stream. No obvious change in morphology and structure is observed after 100 h of stability test (Fig. S3B), demonstrating an effective and stable catalyst.

To give a deep insight into the mechanism of cooperative catalysis, CO_2 methanation over Ni/CNT and Ni/MgAl-MMO catalyst was further investigated by steady-state isotope transient kinetic analysis (SSITKA)-type *in-situ* DRIFT infrared spectroscopy. After 60 min of reaction at 170 ℃, CO_2 was replaced by the isotopic gas ($^{13}CO_2$) for another 60 min of reaction. By correlating the buildup/decay of various surface species including CO, hydrocarbonate and carbonate, detailed information on the catalytic reaction mechanism can be obtained. Fig. 7A shows that once the reaction gas mixture is introduced, typical signals for the gas phase CO_2 (2361 and 2343 cm^{-1}), carbonate (1392 cm^{-1}) and hydrocarbonate (1662 cm^{-1}) are identified immediately over the Ni/MgAl-MMO catalyst. These bands are almost saturated over 60 min. No obvious signal assigned to CH_4 (3016 cm^{-1}) is observed, probably due to the weak adsorption on the catalyst surface. When the $^{12}CO_2$ stream is switched to $^{13}CO_2$ gas, significant changes occur in the DRIFT spectra (Fig. 7B). The bands of $^{12}CO_{2,gas}$ diminish gradually; while new bands attributed to $^{13}CO_{2,gas}$ (2295, 2278 and 2267 cm^{-1}) are observed. The characteristic bands of carbonate (1392 cm^{-1}) and hydrocarbonate (1662 cm^{-1}) display a similar decrease as $^{12}CO_{2,gas}$; while the corresponding new bands due to

Catalysis Science & Technology Accepted Manuscript

^{13}C-carbonate (1317 cm^{-1}) and ^{13}C-hydrocarbonate (1624 cm^{-1}) grow steadily. This indicates that carbonate and hydrocarbonate are intermediates in the main reaction path. In contrast, in the case of Ni/CNT catalyst without base site, the formation of any relevant intermediates during the introduction of feed gas is hardly observed (Fig. 7C and 7D). The results above indicate that the activation of CO_2 molecule to carbonate/hydrocarbonate species is critical for CO_2 methanation, which is achieved by MgO base sites. Although CO_2 is very chemically stable, base sites can activate it to carbonate/hydrocarbonate species at appreciable rates, which has been confirmed by previous studies on pure alkaline supports.[5b,7] It is reported that metal catalysts provide reactive H-species (through H_2 activation) to hydrogenate the carbonate at a temperature far below the uncatalyzed hydrogenation temperature.[7] Therefore, a cooperative catalytic mechanism is proposed for alkaline-assisted Ni-based catalyst, in which Ni site and base site serve as active centers toward H_2 activation (dissociation of H_2) and CO_2 activation, respectively, followed by the subsequent hydrogenation to give methane. Notably, the spillover of dissociated H on MgO surface is rather difficult, according to the valence band theory in which a hydrogen atom does not bond to a solid surface with saturated atoms (*e.g.*, MgO, SiO_2 and Al_2O_3)[19]. It is thus proposed that Ni/MgO interfacial sites act as the dual active centers to cooperatively catalyze the conversion of CO_2 to methane. Moreover, among the four $Ni_x/Mg_{2-x}Al$-MMO samples, the Ni/MgAl-MMO catalyst (molar ratio of Ni/Mg close to 1:1) shows a moderate active site density (as shown in Table 1), which likely induces the optimal tradeoff between H_2 activation and CO_2 activation. This promotes the subsequent hydrogenation of carbonate species to produce methane, and the highest activity is therefore obtained over Ni/MgAl-MMO.

4. Conclusions

In summary, highly-dispersed Ni catalysts supported on the MgO-Al_2O_3 mixed metal oxides were successfully synthesized *via* the topotactic transformation of $Ni_xMg_{2-x}Al$-LDH precursors with various Ni/Mg molar ratios. The resulting $Ni_x/Mg_{2-x}Al$-MMO catalysts are evaluated by the hydrogenation of CO_2 to methane, and the sample of Ni/MgAl-MMO shows largely enhanced catalytic behavior (CO_2 conversion: 97.9%, CH_4 selectivity: 97.5%, reaction temperature: 250 ℃). Both the kinetic study and the time-resolved DRIFTS measurements equipped with SSITKA demonstrate that the base site of MgO serves as active center to activate CO_2 to carbonate/hydrocarbonate. Therefore, a cooperative catalytic mechanism occurring at the Ni species/MgO interface is proposed for this alkaline-assistant Ni-based catalyst, which is optimized in the Ni/MgAl-MMO catalyst, accounting for its excellent low-temperature activity toward CO_2 methanation.

Acknowledgements

This work was supported by the 973 Program (Grant No. 2014CB932104), the National Natural Science Foundation of China, the Fundamental Research Funds for the Central Universities (YS 1406) and the Research on the Chemical Industry Cluster and the Socioeconomic Coordinated Development of Xinjiang (Grant no. JX20140015).

Notes and references

1. (a) J. M. Bermúdez, B. Fidalgo, A. Arenillas and J. A. Menéndez, *Fuel*, 2012, **94**, 197–203; (b) R. Razzaq, H. W. Zhu, L. Jiang, U. Muhammad, C. S. Li and S. J. Zhang, *Ind. Eng. Chem. Res*., 2013, **52**, 2247–2256; (c) Z. F. Qin, J. Ren, M. Q. Miao, Z. Li, J. Y. Lin and K. C. Xie, *Appl. Catal. B-Environ*., 2015, **164**, 18–30.
2. (a) W. Wang, S. P. Wang, X. B. Ma and J. L. Gong, *Chem. Soc. Rev*., 2011, **40**, 3703–3727; (b) P. Gao, F. Li, F. K. Xiao, N. Zhao, N. N. Sun, W. Wei, L. S. Zhong and Y. H. Sun, *Catal. Sci. Technol*., 2012, **2**, 1447–1454; (c) J. Liu, C. M. Li, F. Wang, S. He, H. Chen, Y. F. Zhao, M. Wei, D. G. Evans and X. Duan, *Catal. Sci. Technol*., 2013, **3**, 2627–2633; (d) S. Sharma, Z. P. Hu, P. Zhang, E. W. McFarland and H. Metiu, *J. Catal*., 2011, **278**, 297–309.
3. (a) R. G. Zhang, H. Y. Liu, B. J. Wang and L. X. Ling, *Appl. Catal. B-Environ*., 2012, **126**, 108–120; (b) D. C. Upham, A. R. Derk, S. Sharma, H. Metiu and E. W. McFarland, *Catal. Sci. Technol*., 2015, **5**, 1783–1791; (c) A. Karelovic and P. Ruiz, *ACS Catal*., 2013, **3**, 2799–2812; (d) M. A. A. Aziz, A. A. Jalil, S. Triwahyono, R. R. Mukti, Y. H. Taufiq-Yap and M. R. Sazegar, *Appl. Catal. B-Environ*., 2014, **147**, 359–368; (e) Q. S. Pan, J. X. Peng, S. Wang and S. D. Wang, *Catal. Sci. Technol*., 2014, **4**, 502–509.
4. (a) A. Westermann, B. Azambre, M. C. Bacariza, I. Graça, M. F. Ribeiro, J. M. Lopes and C. Henriques, *Appl. Catal. B-Environ*., 2015, **174**, 120–125; (b) H. Takano, H. Shinomiya, K. Izumiya, N. Kumagai, H. Habazaki and K. Hashimoto, *Int. J. Hydrogen Energ*., 2015, **40**, 8347–8355; (c) W. L. Zhen, B. Li, G. X. Lu and J. T. Ma, *Chem. Commun*., 2015, **51**, 1728–1731; (d) A. Borgschulte, E. Callini, N. Stadie, Y. Arroyo, M. D. Rossell, R. Erni, H. Geerlings, A. Züttel and D. Ferri, *Catal. Sci. Technol*., 2015, **5**, 4613–4621; (e) M. A. A. Aziz, A. A. Jalil, S. Triwahyono and A. Ahmad, *Green. Chem*., 2015, **17**, 2647–2663.
5. (a) Q. S. Pan, J. X. Peng, T. J. Sun, S. Wang and S. D. Wang, *Catal. Commun*., 2014, **45**, 74–78; (b) J. Park and E. W. McFarland, *J. Catal*., 2009, **266**, 92–97; (c) M. Guo and G. X. Lu, *RSC Adv*., 2014, **4**, 58171–58177; (d) Y. R. Li, G. X. Lu and J. T. Ma, *RSC Adv*., 2014, **4**, 17420–17428.
6. (a) A. F. Gusovius and R. Prins, *J. Catal*., 2002, **211**, 273–277; (b) L. F. Liotta, G. Deganello, P. Delichere, C. Leclercq and G. A. Martin, *J. Catal*., 1996, **164**, 334–340; (c) M. J. Climent, A. Corma, S. Iborra, K. Epping and A. Velty, *J. Catal*., 2004, **225**, 316–326; (d) B. Veldurthy, J. M. Clacens and F. Figueras, *J. Catal*., 2005, **229**, 237–242.
7. H. Y. Kim, H. M. Lee and J. N. Park, *J. Phys. Chem. C*, 2010, **114**, 7128–7131.
8. (a) Q. Wang and D. O'Hare, *Chem. Rev*., 2012, **112**, 4124–4155; (b) C. M. Li, M. Wei, D. G. Evans and X. Duan, *Small*, 2014, **10**, 4469–4486; (c) J. Liang, R. Ma, N. Iyi, Y. Ebina, K. Takada and T. Sasaki, *Chem. Mater*., 2010, **22**, 371–378.
9. (a) J. A. Gursky, S. D. Blough, C. Luna, C. Gomez, A. N. Luevano and E. A. Gardner, *J. Am. Chem. Soc*., 2006, **128**, 8376–8377; (b) S. He, C. M. Li, H. Chen, D. S. Su, B. S. Zhang, X. Z. Cao, B. Y. Wang, M. Wei, D. G. Evans and X. Duan, *Chem. Mater*., 2013, **25**, 1040–1046; (c) J. Liu, S. M. Xu, W. H. Bing, F. Wang, C. M. Li, M. Wei, D. G. Evans and X. Duan, *ChemCatChem*, 2015, **7**, 846–855; (d) H. C. Liu and E. Min, *Green Chem*., 2006, **8**, 657–662; (e) R. D. Hetterley, R. Mackey, J. T. A. Jones, Y. Z. Khimyak, A. M. Fogg and L. V. Kozhevnikov, *J. Catal*., 2008, **258**, 250–255.
10. Y. Zhao, F. Li, R. Zhang, D. G. Evans and X. Duan, *Chem. Mater*., 2002, **14**, 4286–4291.
11. J. Pisson, C. Taviot-Gueho, Y. Israeli, F. Leroux, P. Munsch, J. P. Itie, V. Briois, N. Morel-Desrosiers and J. P. Besse, *J. Phys. Chem. B*, 2003, **107**, 9243–9248.
12. F. Z. Zhang, J. L. Chen, P. Chen, Z. Y. Sun and S. L. Xu, *AIChE J*., 2012, **58**, 1853–1861.
13. (a) C. Zhao, Y. Z. Yu, A. Jentys and J. A. Lercher, *Appl. Catal., B-Environ*., 2013, **132**, 282–292; (b) B. Mile, D. Stirling, M. A. Zammitt, A. Lovell and M. Webb, *J. Catal*., 1988, **114**, 217–229.
14. Z. L. Yuan, L. N. Wang, J. H. Wang, S. X. Xia, P. Chen, Z. Y. Hou and X. M. Zheng, *Appl. Catal. B-Environ*., 2011, **101**, 431–440.
15. (a) Y. Lee and S. Oyama, *J. Catal*., 2006, **239**, 376–389; (b) S.

Catalysis Science & Technology Accepted Manuscript

Derrouiche and D. Bianchi, *Appl. Catal. A*, 2006, **313**, 208–217.
16. (a) J. H. Kwak, L. Kovarik and J. Szanyi, *ACS Catal*., 2013, **3**, 2094–2100; (b) G. D. Lee, M. J. Moon, J. H. Park, S. S. Park and S. S. Hong, *Korean J. Chem. Eng*., 2005, **22**, 541–546; (c) N. Perkas, G. Amirian, Z. Y. Zhong, J. Teo, Y. Gofer and A. Gedanken, *Catal. Lett*., 2009, **130**, 455–462.
17. (a) P. C. Zonetti, S. Letichevsky, A. B. Gaspar, E. F. Sousa-Aguia and L. G. Appel, *Appl. Catal. A*, 2014, **475**, 48–54; (b) H. C. Wu, Y. C. Chang, J. H. Wu, J. H. Lin, I. K. Linc and C. S. Chen, *Catal. Sci. Technol*., 2015, **5**, 4154–4163.
18. (a) A. Yamaguchi and E. Iglesia, *J. Catal*., 2010, **274**, 52–63; (b) J. Bradford and M. A. Vannice, *J. Catal*., 1999, **183**, 69–75.
19. (a) E. A. Colbourn and W. C. Mackrodt, *Surf. Sci*., 1982, **117**, 571–580; (b) S. P. Karna, R. D. Pugh, W. M. Shedd and B. K. Singaraju, *J. Non-Cryst. Solids*, 1999, **254**, 66–73; (c) F. Ahmed, M. K. Alam, A. Suzuki, M. Koyama, H. Tsuboi, N. Hatakeyama, A. Endou, H. Takaba, C. A. Del Carpio, M. Kubo and A. Miyamoto, *J. Phys. Chem. C*, 2009, **113**, 15676–15683.

Catalysis Science & Technology Accepted Manuscript

Supporting Information for

Alkaline-assisted Ni nanocatalysts with largely enhanced low-temperature activity toward CO_2 methanation

Jie Liu,[a] Weihan Bing,[a] Xiaoge Xue,[a] Fei Wang,[a] Bin Wang,[b] Shan He,*[a] Yingkui Zhang,[a] Min Wei*[a]

[a] *State Key Laboratory of Chemical Resource Engineering, Beijing University of Chemical Technology, Beijing 100029, P. R. China*

[b] *Beijing Research Institute of Chemical Industry, Sinopec Group, Beijing 100013, P. R. China*

Graphical Abstract

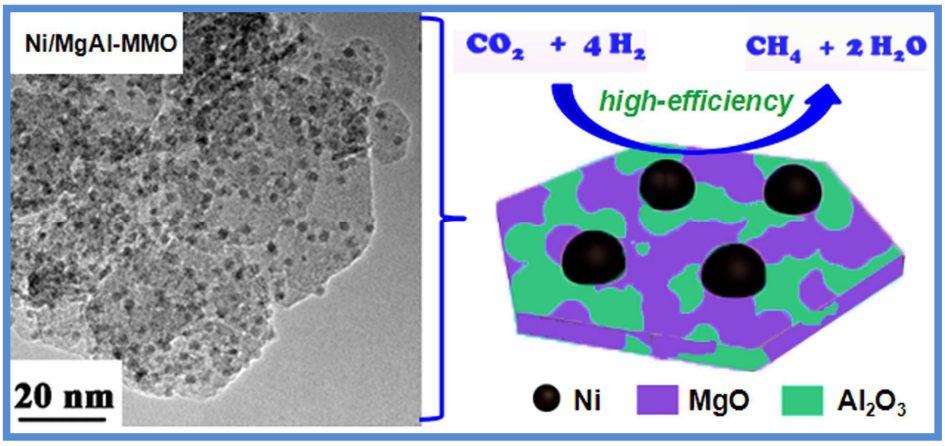

Alkaline-assisted Ni/MgAl-MMO catalyst derived from NiMgAl-LDH precursor exhibits excellent catalytic behavior towards CO_2 methanation.

Catalysis Science & Technology Accepted Manuscript